Incorporation of Outer Membrane Protein OmpG in Lipid Membranes: Protein−lipid Interactions and β-Barrel Orientation†

V. Anbazhagan,‡ J. Qu,§ J. H. Kleinschmidt,*,§ and D. Marsh*,‡

Max-Planck-Institut für biophysikalische Chemie, Abt. Spektroskopie, 37070 Göttingen, Germany, and University of Konstanz, Fachbereich Biologie, 78457 Konstanz, Germany

Received February 4, 2008; Revised Manuscript Received April 7, 2008

ABSTRACT: OmpG is an intermediate size, monomeric, outer membrane protein from *Escherichia coli*, with $n_\beta = 14$ β-strands. It has a large pore that is amenable to modification by protein engineering. The stoichiometry ($N_b = 20$) and selectivity ($K_r = 0.7-1.2$) of lipid−protein interaction with OmpG incorporated in dimyristoyl phosphatidylcholine bilayer membranes was determined with various 14-position spin-labeled lipids by using EPR spectroscopy. The limited selectivity for different lipid species is consistent with the disposition of charged residues in the protein. The conformation and orientation (β-strand tilt and β-barrel order parameters) of OmpG in disaturated phosphatidylcholines of odd and even chain lengths from C(12:0) to C(17:0) was determined from polarized infrared spectroscopy of the amide I and amide II bands. A discontinuity in the protein orientation (deduced from the β-barrel order parameters) is observed at the point of hydrophobic matching of the protein with lipid chain length. Compared with smaller (OmpA; $n_\beta = 8$) and larger (FhuA; $n_\beta = 22$) monomeric *E. coli* outer membrane proteins, the stoichiometry of motionally restricted lipids increases linearly with the number of β-strands, the tilt ($\beta \sim 44°$) of the β-strands is comparable for the three proteins, and the order parameter of the β-barrel increases regularly with n_β. These systematic features of the integration of monomeric β-barrel proteins in lipid membranes could be useful for characterizing outer membrane proteins of unknown structure.

OmpG is a 14-stranded, all nearest neighbor, β-barrel protein that is normally expressed only at trace levels in the outer membrane of *Escherichia coli* (*1, 2*). The protein is monomeric (*3*) and, unlike the other monomeric outer membrane proteins such as FhuA that have large pores, the lumen of the barrel is not occupied by an additional cork domain, nor does it have the eyelet constriction of the classical trimeric porins, such as OmpF. OmpG facilitates the uptake of sugars when the main sugar porins, such as LamB, either are not present or are disabled (*4*). The nonselective pore for mono-, di-, and trisaccharides is unconstricted and has a limiting diameter of 2 nm (*5*). Gating induced by changes in pH is thought to involve one of the extracellular loops that connect adjacent β-strands folding over the channel entrance (*2*). From these points of view, OmpG is an attractive candidate for protein engineering studies on channel function of site-specific mutants and the development of biosensors (*6*).

In previous studies of monomeric β-barrel proteins, we have determined the stoichiometry and selectivity of lipid−protein interactions with the 8-stranded outer membrane protein OmpA and the 22-stranded ferrichrome-iron receptor FhuA by using spin-label EPR[1] spectroscopy (*7*), and have studied the orientation and conformation of these proteins in membranes by using polarized infrared spectroscopy (*8*). These methods provide essential information on the way in which β-barrel proteins integrate in the lipid membrane and how this depends on different lipid species (*9*−*11*). The size of the protein influences both the stoichiometry of lipids associated with the membrane−penetrant surface (*12*) and the extent of tilt of the β-barrel relative to the membrane director (*13*). It is thus of direct interest to determine the membrane properties of a monomeric β-barrel that is intermediate in size between those that have been studied so far. This is done in the present work by performing similar studies on OmpG, which we have reconstituted in phospholipid bilayers. In this way, we are able to establish correlations between the membrane interactions and protein size that may be used in the future to gain information on outer membrane proteins that are not so well characterized.

† V.A. is supported by a fellowship from the Alexander von Humboldt Foundation. This work was supported in part by Grant TP B3 of TR-SFB 11 of the Deutsche Forschungsgemeinschaft to J.H.K.

* Corresponding authors. Tel: +49 551 1285. Fax: +49 551 1501. E-mail: dmarsh@gwdg.de (D.M.); Tel: +49 7531 88 2291. E-mail: joerg.helmut.kleinschmidt@uni-konstanz.de (J.H.K.).

‡ Max-Planck-Institut für biophysikalische Chemie.

§ University of Konstanz.

[1] Abbreviations: EPR, electron paramagnetic resonance; 14-PCSL, -PASL, -PGSL, and -PESL, 1-acyl-2-[14-(4,4-dimethyloxazolidinyl-*N*-oxyl)]stearoyl-*sn*-glycero-3- phosphocholine, -phosphatidic acid, -phosphoglycerol, and -phosphoethanolamine; 14-DGSL, 1-acyl-2-[14-(4,4′-dimethyloxazolidinyl-*N*-oxyl)]stearoyl-*sn*-glycerol; 14-SASL, 14-(4,4-dimethyloxazolidinyl-*N*-oxyl)stearic acid; ATR, attenuated total reflectance; FTIR, Fourier transform infrared; IPTG, isopropyl-β-D-thiogalactopyranoside; Tris, tris(hydroxymethyl)-aminomethane; Hepes, *N*-(2-hydroxyethyl)piperazine-*N*′-2-ethanesulphonic acid; EDTA, ethylenediaminetetraacetic acid; OBG, *n*-octyl β-D-glucopyranoside; SDS−PAGE, polyacrylamide gel electrophoresis in sodium dodecyl sulfate.

10.1021/bi800203g CCC: $40.75 © 2008 American Chemical Society
Published on Web 05/13/2008

MATERIALS AND METHODS

Materials. Spin-labeled stearic acid, 14-SASL, was synthesized according to ref *14*. Spin-labeled phosphatidylcholine, 14-PCSL, was synthesized by acylation of lysophosphatidylcholine with 14-SASL, as described in ref *15*. Other spin-labeled phospholipids, 14-PGSL, 14-PESL, and 14-PASL, were prepared from 14-PCSL by headgroup exchange mediated by phospholipase D (*15*). Symmetrical, disaturated phosphatidylcholines, diC(n_C:0)PtdCho, with odd and even chain lengths from $n_C = 12$ to 17 were obtained from Avanti Polar Lipids (Alabaster, AL). All other chemicals were from Sigma Chemical Co. (St. Louis, MO).

Isolation of OmpG. For overexpression and isolation of OmpG, the *ompG* gene was amplified by PCR (60 °C annealing temperature), using 50 ng of *E. coli* MG1655 genomic DNA as template. To eliminate the signal sequence, the oligonucleotide primers 5′-TAGGGCCATATGGAGGAAAGGAACGACTGG-3′ and 5′-CTACTCGAGTCAAAGCTTGAACGAGTAATTTACGCCG-3′ were used, and the PCR product was cloned into the pET29b vector (Novagen) using the NdeI and XhoI restriction sites, yielding plasmid pET29OmpGm2 (*16*). pET29OmpGm2 was transformed into *E. coli* BL21(DE3) (Stratagene) to express OmpG in the form of inclusion bodies. Cells were grown in 2xYT medium to $A_{600nm} \cong 0.8$, and expression was induced by addition of IPTG to a final concentration of 0.5 mM for 3 h at 37 °C. After harvesting by centrifugation at 8000 rpm for 30 min at 4 °C, the cells were resuspended in TBS-I buffer (20 mM Tris, 100 mM NaCl, 0.1% β-mercaptoethanol at pH 8.0). Solutions of 0.5 mg of lysozyme and 4 mg of sodium cholate were added per 1 g of cells at room temperature, and the cells were subsequently disrupted by using a Branson Ultrasonifer W-450 D with macrotip in an ice−water bath for 30 min. The insoluble inclusion bodies of OmpG were obtained by centrifugation for 30 min at 8000 rpm, at 4 °C. The inclusion bodies were washed thoroughly with TBS-II (20 mM Tris, 100 mM NaCl, 0.1% β-mercaptoethanol, 1% Triton X-100, 1 M urea at pH 8.0) and TBS-III (20 mM Tris, 100 mM NaCl, 0.1% β-mercaptoethanol, 1 M urea at pH 8.0) buffer, respectively. The inclusion bodies were then dissolved in TBS-IV (20 mM Tris, 100 mM NaCl, 0.1% β-mercaptoethanol, 8 M urea at pH 8.0). The solubilized protein was loaded onto a Q-sepharose column that was pre-equilibrated with Tris-IV buffer, and unfolded OmpG was eluted by means of a 0−100 mM NaCl gradient. Refolding of OmpG was achieved by dilution in 4% (wt/vol) *n*-octyl β-D-glucopyranoside (OBG), to a final urea concentration of 1.5 M, followed by incubation at 37 °C for 5 h. Refolding was monitored by SDS−PAGE, taking advantage of the difference in apparent molecular masses of refolded (28 kDa) and unfolded (36 kDa) OmpG, when samples were not boiled prior to electrophoresis (*3*). Protein concentrations were determined by the method of Lowry et al. (*17*), using bovine serum albumin as a standard.

Reconstitution of OmpG into Membranes. Phospholipid solutions containing 1 mol % of the desired spin-labeled lipid were prepared in $CHCl_3$ and dried under a stream of dry nitrogen gas. The resulting lipid film was desiccated overnight under vacuum and then covered with argon. The dry lipid film was hydrated with 20 mM Tris, 4% OBG, and 1.5% urea at pH 8.0 to obtain detergent-solubilized liposomes. Reconstitution was carried out by mixing 1 mg of the above lipid vesicles with protein refolded in OBG to achieve the desired lipid−protein ratio. The sample was mixed well and incubated overnight at 37 °C. Detergent removal was achieved by extensive dialysis at 8 °C against 10 mM Hepes buffer at pH 7.2 containing 2 mM EDTA and 250 mM NaCl, using 10-kDa cutoff dialysis membranes. Six to eight changes of 2 L of buffer were made every 7−8 h, with the last dialysis step extending overnight.

Electron Spin Resonance Spectroscopy. ESR spectra were recorded on a 9-GHz Bruker EMX EPR spectrometer with a model ER 041 XK-D microwave bridge. Samples were placed in 50 μL glass capillaries and flame sealed. The capillaries were placed in a standard 4 mm quartz sample tube containing light silicone oil for thermal stability. The temperature of the sample was maintained constant by blowing thermostatted nitrogen gas through a quartz dewar. Spectra were recorded using the following instrumental settings: sweep width, 100 G; resolution, 1024 points; time constant, 20.5 ms; sweep time, 42 s; modulation frequency, 100 kHz; modulation amplitude, 1.0 G; incident power, 5 mW. Spectral subtraction or addition and integration were performed as described in ref *18*. Spectral reference libraries for the fluid and motionally restricted components were obtained from 14-PCSL in egg phosphatidylcholine dispersions and in sonicated diC(14:0)PtdCho small unilamellar vesicles, respectively, at various temperatures.

ATR Spectroscopy. OmpG was purified and reconstituted as described above. The reconstituted sample was layered on a clean ZnSe ATR crystal. Initially, the sample was dried with dry nitrogen purge and then desiccated overnight with a vacuum pump. The dry lipid film was incubated in a Bruker IFS 25 FTIR spectrometer by purging with dry nitrogen at 1.5 kp/cm^2 pressure. ATR spectra were recorded at a nominal resolution of 2 cm^{-1} with polarization parallel (0°) and perpendicular (90°) to the plane of the incident beam. All instrumental settings, other than that of the polarizer, were maintained constant when recording the 0° and 90° spectra. The sample was then hydrated with an excess of 10 mM Hepes at pH 7.2 buffer containing 2 mM EDTA and 250 mM NaCl, prepared in D_2O, and washed (using a pipet) again with the same buffer in order to remove noninserted lipid and protein. Meanwhile, ATR spectra were recorded at both polarizations for every wash. The specially constructed ATR sample holder was hermetically sealed, and temperature was controlled using a recirculating water bath. Spectra were recorded both in the gel phase (∼10° below the lipid chain melting temperature) and in the fluid phase (∼10° above the lipid chain melting temperature) of the membranes. Further details of the ATR spectroscopy are given in ref *19*.

To determine the dichroic ratio, each spectrum was analyzed using the Peak Fitting Module (PFM) of Origin Pro 7 (Microcal Software, Hampton, MA). If necessary, spectra were smoothed with 11-point Savitsky−Golay smoothing to remove the noise from residual water vapor. A local baseline was established, and band fitting using the Levenberg−Marquardt algorithm was carried out from 1500 to 1710 cm^{-1} and from 1590 to 1690 cm^{-1} for dry and hydrated samples, respectively. Lorentzian bandshapes were used with the component bands, except for the major 1625 cm^{-1} component band of the hydrated sample, which was Gaussian. The absorption intensity ratios for parallel and

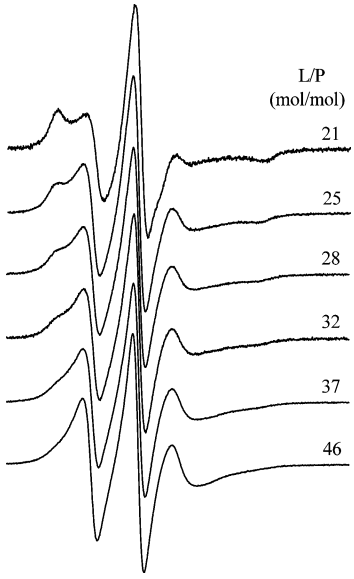

FIGURE 1: EPR spectra of phosphatidylcholine spin labeled on the 14-C atom of the *sn*-2 chain (14-PCSL) in dimyristoyl phosphatidylcholine (diC(14:0)PtdCho) membranes containing OmpG at the lipid/protein mole ratios (L/P) indicated in the figure. $T = 30$ °C; total scan width = 100 G.

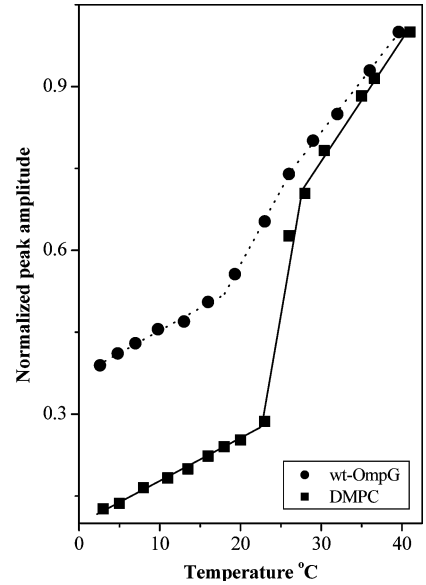

FIGURE 2: Temperature dependence of the central line height in the EPR spectra of the 14-PCSL spin label in diC(14:0)PtdCho membranes containing OmpG at a lipid/protein ratio of 32 mol/mol (●) and in diC(14:0)PtdCho alone (■).

perpendicular polarization were taken as the ATR dichroic ratio (R), using the intensities obtained at 1625−1630 and 1530 cm^{-1} from the curve-fitting analysis for the amide I and amide II bands, respectively. These component bands had the same positions and widths in the parallel and perpendicular polarizations. The dichroic ratio was essentially unchanged when fitting was performed with a Gaussian band shape for the component at 1630 cm^{-1} of the dry sample, instead of a Lorentzian band shape. (The resulting Gaussian bandwidths, 26−27 cm^{-1}, were comparable to those of the hydrated samples.) The dichroic ratio changes with the first two to three washes and then becomes stable, which is taken to correspond to the respective aligned hydrated samples. To calculate molecular orientations from dichroic ratios, intensities of the infrared electric field components were obtained from the thick film approximation: $E_x^2/E_y^2 = 0.450$ and $E_z^2/E_y^2 = 1.550$ for a 45°-cut ZnSe ATR crystal.

RESULTS

Lipid Spin-Label EPR. Figure 1 shows the EPR spectra of spin-labeled phosphatidylcholine, 14-PCSL, in reconstituted bilayers of dimyristoyl phosphatidylcholine (diC(14:0)PtdCho) that contain OmpG at different lipid/protein ratios, as indicated. The spectra are recorded at 30 °C, i.e., in the fluid phase of diC(14:0)PtdCho lipid bilayers. Figure 2 shows gel−fluid phase transition curves for diC(14:0)PtdCho bilayers in the presence and absence of OmpG. These confirm that OmpG/diC(14:0)PtdCho membranes are still in the fluid phase at 30 °C, at protein/lipid ratios up to 1:32 mol/mol.

All the EPR spectra in Figure 1 consist of two components, a sharp and a broad one, that are, respectively, characteristic of lipids in fluid bilayer regions of the membrane and of lipids that are motionally restricted at the intramembrane surface of the protein (see, e.g., refs *20*−*23*). For α-helical proteins these two lipid populations are not static, but exchange with rates ∼10^6−10^7 s^{-1} (*24*−*27*), which are slow on the time scale of conventional spin-label EPR and less than lipid translational diffusion rates (*28, 29*), but are rapid on the time scale of NMR measurements (*9, 11, 30*).

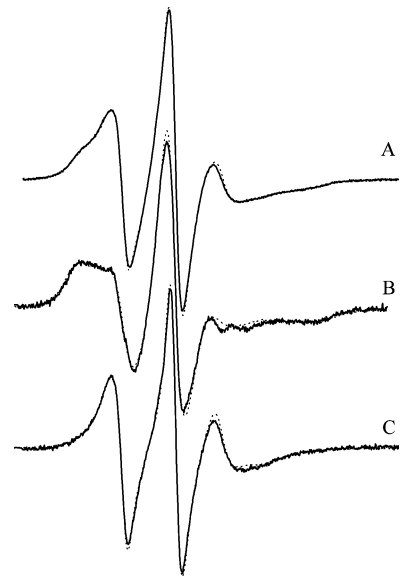

FIGURE 3: Spectral subtractions to quantitate the relative proportions of the fluid [fraction, $(1 - f_b)$] and motionally restricted [fraction, f_b] components from the EPR spectra of 14-PCSL in OmpG/diC(14:0)PtdCho membranes. (A) Solid line: experimental spectrum from OmpG/diC(14:0)PtdCho 1:32 mol/mol membranes at 30 °C. Dotted line: summed spectrum from addition of the dotted-line spectra in B and C. (B) Solid line: difference spectrum obtained by subtracting the dotted-line spectrum given in C from the solid-line spectrum in A. Dotted line: motionally restricted comparison spectrum (sonicated diC(14:0)PtdCho vesicles at 9 °C). (C) Solid line: difference spectrum obtained by subtracting the dotted-line spectrum given in B from the solid-line spectrum in A. Dotted line: fluid comparison spectrum (egg phosphatidylcholine dispersion at 8 °C).

Figure 3 shows how the two-component EPR spectra are analyzed by using spectral subtraction or addition to yield the relative proportions of the two spin-labeled lipid populations. A subtraction end point that yields the spectral

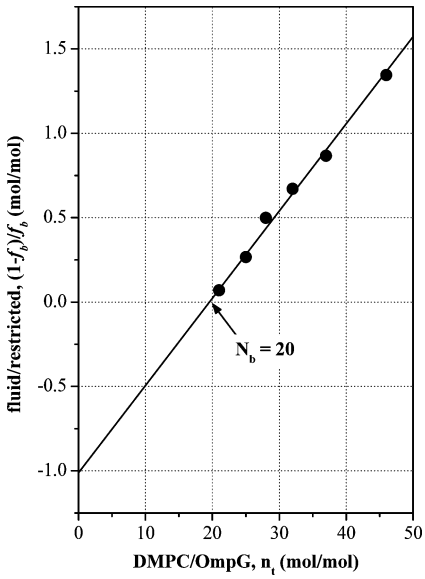

FIGURE 4: Dependence of the ratio of fluid to motionally restricted populations, $(1 - f_b)/f_b$, of 14-PCSL spin label on the lipid/protein ratio, n_t, in diC(14:0)PtdCho membranes containing OmpG (●). The solid line is a linear regression, giving an intercept of $K_r = 1.0$.

component arising only from the motionally restricted lipids (Figure 3B), reveals that $1 - f_b = 34\%$ of the total intensity must be removed from the original spectrum (Figure 3A) by using a single fluid component. Correspondingly, the complementary subtraction (Figure 3C) requires subtraction of $f_b = 67\%$ of the total intensity by using a motionally restricted single component.

Figure 4 shows the results of analyzing the spectral data in Figure 1 according to the method shown in Figure 3, including also spectral addition (dotted line in Figure 3A) with least-squares minimization. The dependence on lipid/protein ratio, n_t, is plotted according to the standard expression for equilibrium exchange association with the protein of spin-labeled lipids at probe concentrations (*31*):

$$(1 - f_b)/f_b = (n_t/N_b - 1)/K_r \quad (1)$$

where N_b is the number of lipid association sites at the intramembranous surface of the protein, and K_r is the relative association constant of the spin-labeled 14-PCSL lipid, referred to the unlabeled diC(14:0)PtdCho host lipid. The linear regression in Figure 4, according to eq 1, indicates a fixed stoichiometry of $N_b = 19.6 \pm 1.0$ lipid sites per OmpG, and an association constant of spin-labeled phosphatidylcholine relative to diC(14:0)PtdCho of $K_r = 1.0$.

Figure 5 shows the EPR spectra of different spin-labeled lipid species in OmpG/diC(14:0)PtdCho membranes of identical lipid/protein ratio. The similarity of the two-component spectra from the different phospholipid species indicates only limited selectivity of the different lipid polar headgroups for interaction with OmpG. For a fixed lipid/protein ratio, n_t, the ratio of relative association constants is given by:

$$K_r/K_r^{PC} = (1/f_b^{PC} - 1)/(1/f_b - 1) \quad (2)$$

where f_b^{PC} is the fraction of motionally restricted, spin-labeled phosphatidylcholine, and f_b is that of the lipid in question. Values of the selectivity ratio, K_r/K_r^{PC}, for the different lipids that are obtained from the data of Figure 5 by using eq 2 are given in Table 1. With the exception of diacylglycerol (14-DGSL), which probably has a different vertical location in the membrane (*32*), all lipids tested have relative association constants that are close to that of phosphatidylcholine (14-PCSL).

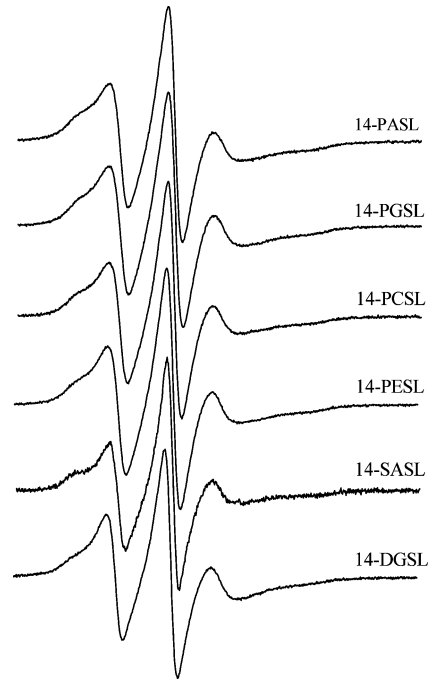

FIGURE 5: ESR spectra of spin-labeled phospholipids (14-PXSL) with different polar headgroups and of the corresponding spin labeled diacylglycerol (14-DGSL) and stearic acid (14-SASL) in diC(14:0)PtdCho membranes containing OmpG at a fixed lipid/protein ratio of 32 mol/mol. $T = 30$ °C; total scan width = 100 G.

Table 1: Fraction (f_b) of Motionally Restricted Spin-Labeled Lipid and Relative Association Constants, K_r, Normalized to That for Phosphatidylcholine (K_r^{PC}), Obtained by Spectral Addition for the EPR Spectra of Different Spin Labels in diC(14:0)PtdCho/OmpG Membranes of Lipid/Protein Ratio 32 mol/mol

spin label	motionally restricted fraction (f_b)	K_r/K_r^{PC}	$\Delta G - \Delta G^{PC}$ (kJ/mol)[a]
14-PASL	0.64	1.2	−0.44
14-PGSL	0.63	1.1	−0.34
14-PESL	0.58	0.9	+0.24
14-SASL	0.51	0.7	+0.90
14-DGSL	0.44	0.5	+1.60
14-PCSL	0.60	1.0	0.0

[a] Free energy of association, relative to 14-PCSL: $\Delta G - \Delta G^{PC} = -RT \ln(K_r/K_r^{PC})$. Temperature = 30 °C.

Polarized IR Spectra of OmpG in PtdCho. Figure 6 shows the amide region from the polarized ATR spectra of OmpG in aligned membranes of dipalmitoyl phosphatidylcholine (diC(16:0)PtdCho). In the dry state (Figures 6A and B), both the amide I and amide II bands are visible, whereas in membranes hydrated with D_2O (Figures 6C and D), the amide II band is shifted to much lower frequencies where it overlaps with bands from the lipid. Band fitting shown in Figure 6 demonstrates the predominant β-sheet content of the protein, with the major band at ca. 1625 cm^{-1} in the amide I region ($\nu_\perp(\pi,0)$ mode), and at ca. 1530−1550 cm^{-1} in the amide II region ($\nu_{//}(0,\pi)$ mode). The minor band at ca. 1670 cm^{-1} in the amide I region ($\nu_{//}(0,\pi)$ mode) from hydrated membranes is characteristic of antiparallel β-sheets

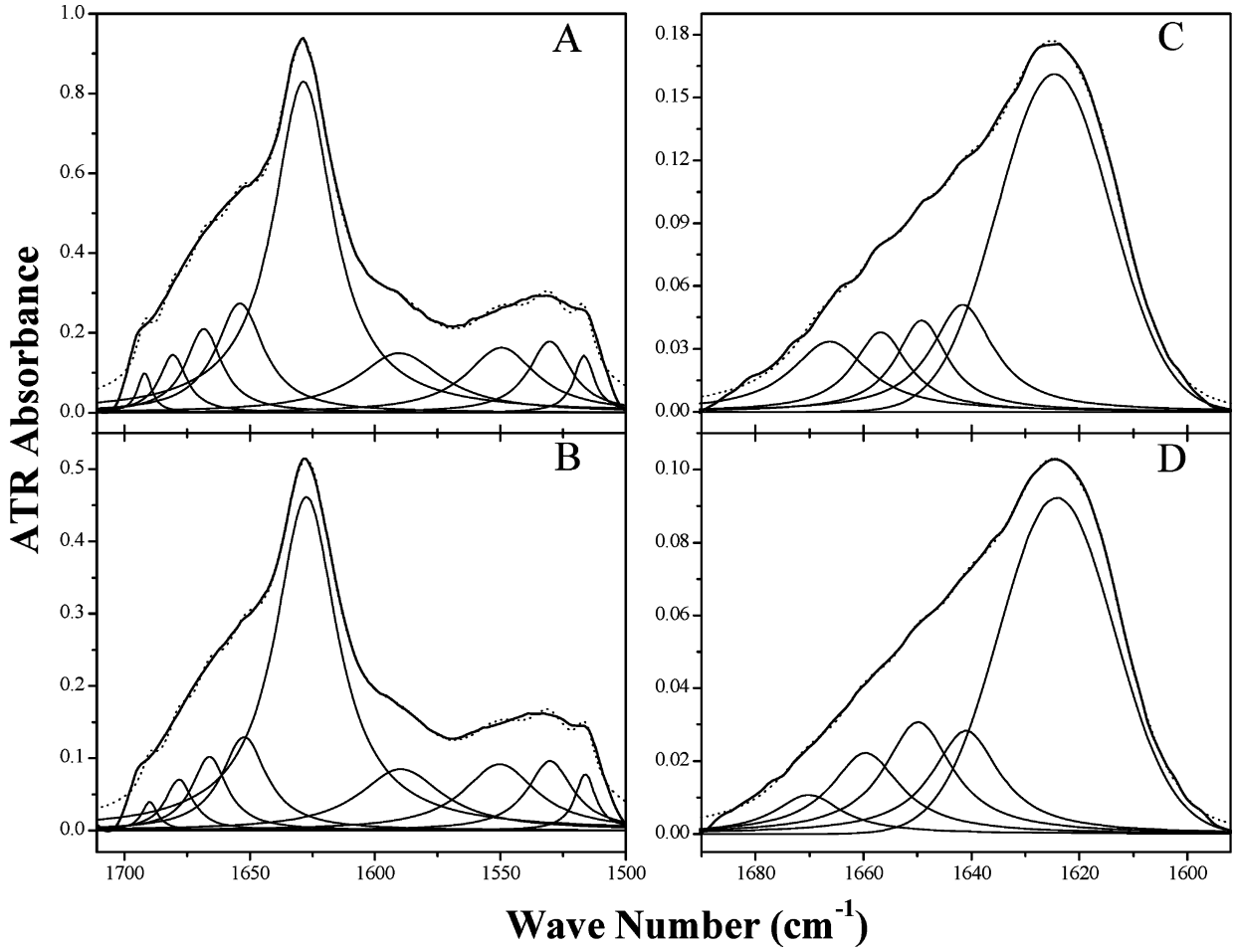

FIGURE 6: Polarized ATR-FTIR spectra of OmpG reconstituted with diC(16:0)PtdCho lipid. Spectra A and B were obtained in the dry state, whereas spectra C and D were obtained in the hydrated gel phase. (T = 32 °C.) The spectra in the upper panels (A and C) correspond to parallel polarization, and those in the lower panels (B and D) correspond to perpendicular polarization of the incident radiation. Note the different ordinate scales. The dotted lines correspond to the least-squares fit, with the bands obtained from the band-fitting analysis shown below the experimental spectrum. The positions and widths at half-height of the major amide I band are (A) 1629 cm^{-1} and 29 cm^{-1} (Lorentzian), (B) 1627 cm^{-1} and 30 cm^{-1} (Lorentzian), (C) 1625 cm^{-1} and 25 cm^{-1} (Gaussian), and (D) 1624 cm^{-1} and 25 cm^{-1} (Gaussian), respectively.

(*33*), as in the all-nearest-neighbor strand connectivity of the OmpG β-barrel (*1, 2*).

Table 2 gives the results of band fitting for the amide I region from OmpG in disaturated phosphatidylcholines of different chain lengths. Fitting data are given for hydrated membranes in the gel and fluid phases, recorded at temperatures 10° below and 10° above the respective chain-melting transitions. The conformational populations are very similar in the fluid and gel phases of a given lipid. The β-sheet population of OmpG in the different phosphatidylcholine host lipids ranges progressively from 68% in C(12:0) to 58% in C(17:0), with a mean value of 63 ± 4%. For comparison, the β-sheet content is 66% to 71% in the different crystal structures of OmpG ((*1, 2*) PDB: 2iww, 2iwv, 2f1c), and 43% in micelles from NMR ((*34*) PDB: 2jqy). Presumably, phosphatidylcholine bilayer membranes provide a more structuring environment than do dodecylphosphocholine micelles. A similar conclusion was reached recently from circular dichroism studies on the human VDAC protein: β-sheet content decreased on adding nonionic detergent to bilayer-reconstituted hVDAC1 channels (*35*).

Amide Dichroism of OmpG in PtdCho. Figure 7 shows the dichroic ratios of the amide I band from OmpG in bilayer membranes hydrated in D_2O, as a function of chain length, n_C, of the disaturated PtdCho. Values are given for membranes in the gel phase and for those in the fluid phase, above the lipid chain-melting temperature. The general trend is an increase in amide I dichroic ratio with increasing lipid chain length. A single dichroic ratio is insufficient to define the orientation of a β-sheet membrane protein because this depends both on the tilt, β, of the strands within the sheet and on the inclination, α, of the sheet to the membrane normal (*13*).

For a β-barrel of large radius (or a flattened barrel), the dichroism can be approximated by that for a planar sheet. The dichroic ratio of the amide I band is then given by (*13*):

$$R_I = \frac{E_x^2}{E_y^2} + \frac{2\langle\cos^2\alpha\rangle\langle\sin^2\beta\rangle}{1-\langle\cos^2\alpha\rangle\langle\sin^2\beta\rangle}\frac{E_z^2}{E_y^2} \quad (3)$$

because the transition moment is oriented perpendicular to the strand axis. On the other hand, the transition moment for the amide II band is oriented along the strand axis and the dichroic ratio is given by:

$$R_{II} = \frac{E_x^2}{E_y^2} + \frac{2\langle\cos^2\alpha\rangle\langle\cos^2\beta\rangle}{1-\langle\cos^2\alpha\rangle\langle\cos^2\beta\rangle}\frac{E_z^2}{E_y^2} \quad (4)$$

Table 2: Band Fitting of the Polarized ATR Spectra from the Amide I Band of OmpG in Hydrated Disaturated Phosphatidylcholines, diC(n_C:0)PtdCho, with Different Chain Lengths, n_C, in the Gel and Fluid Phases

	gel		fluid	
C(n_C:0)	position (cm^{-1})	normalized area (%)[a]	position (cm^{-1})	normalized area (%)[a]
C(12:0)			1627	62
			1642	9
			1648	12
			1657	11
			1667	6
C(13:0)	1627	63	1626	63
	1642	8	1641	11
	1648	12	1649	13
	1657	11	1658	9
	1667	6	1666	4
C(14:0)	1626	61	1625	63
	1643	13	1642	12
	1651	13	1649	12
	1660	9	1658	9
	1669	4	1668	4
C(15:0)	1625	57	1625	57
	1642	16	1642	16
	1651	15	1652	14
	1661	8	1661	9
	1671	4	1671	4
C(16:0)	1624	53	1624	54
	1640	13	1642	13
	1648	15	1649	14
	1658	11	1659	10
	1668	8	1670	9
C(17:0)	1624	50	1624	50
	1640	15	1641	16
	1648	12	1648	11
	1657	16	1658	15
	1667	7	1668	8

[a] Relative band intensities are obtained by combining integrated absorbances, $A_{\parallel}$ and $A_{\perp}$, with radiation polarized parallel and perpendicular, respectively, to the plane of the incident beam. The appropriate combination that reflects the full intensity is $A_{\parallel} + (2E_z^2/E_y^2 - E_x^2/E_y^2)A_{\perp}$ (*53*).

where angular brackets indicate an ensemble average. Combining dichroic ratios from the amide I and amide II bands therefore allows determination of α and β separately. Applying this to the dichroic ratios, R_I and R_{II}, of the dry samples, yields a consistent mean value for the strand tilt of $\beta = 44.0 \pm 0.7°$ ($N = 11$) from measurements in diC(n_C:0)PtdCho with chainlengths from $n_C = 12$ to 17.

Using the mean value of the strand tilt, $\beta = 44.0 \pm 0.7°$, deduced from the dry sample, together with the dichroic ratios for the hydrated samples from Figure 7, yields the values for the order parameter, $\langle P_2(\cos \alpha)\rangle$, and mean tilt, α, of the β-sheets that are given in Table 3. The trend is similar to that of the dichroic ratios: the order parameters increase, and the tilt angles decrease, with increasing lipid chain length.

Lipid Chain Dichroism in OmpG/PtdCho. The order parameters, $\langle P_2(\cos \theta_{ch})\rangle$, of the lipid chains, relative to the substrate normal, are given in Table 4. These values are derived from the dichroic ratios, R_{CH_2}, of the CH_2 symmetric and antisymmetric stretch bands at 2850 cm^{-1} and 2919 cm^{-1}, respectively. The transition moment for CH_2 stretch vibrations is perpendicular to the chain axis, and the order parameter of the latter is related to the dichroic ratio by (see, e.g., *10*):

$$\langle P_2(\cos \theta_{ch})\rangle = \frac{2(E_z^2/E_y^2 + E_x^2/E_y^2 - R_{CH_2})}{2E_z^2/E_y^2 - E_x^2/E_y^2 + R_{CH_2}} \quad (5)$$

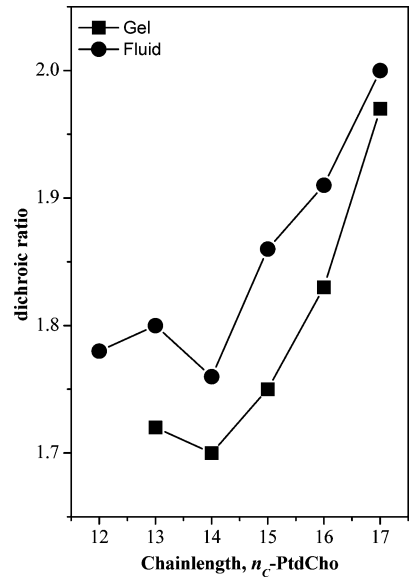

FIGURE 7: Dependence of the dichroic ratios from the amide I band of OmpG on lipid chain length, n_C, of the diC(n_C:0)PtdCho membrane in which the protein is incorporated. Dichroic ratios are given for the samples in the gel phase (■) and in the fluid phase (●). Membranes were hydrated in D_2O buffer.

Table 3: Order Parameters, $\langle P_2(\cos \alpha)\rangle$, and Mean Effective Inclination, α, of the β-Sheets of OmpG Reconstituted in Disaturated Phosphatidylcholines, diC(n_C:0)PtdCho, with Different Chain Lengths, n_C, in the Gel and Fluid Phases[a]

	gel		fluid	
C(n_C:0)	$\langle P_2(\cos \alpha)\rangle$	α (°)	$\langle P_2(\cos \alpha)\rangle$	α (°)
C(12:0)			0.43	38
C(13:0)	0.41	39	0.46	37
C(14:0)	0.41	39	0.43	38
C(15:0)	0.43	38	0.48	36
C(16:0)	0.46	37	0.51	35
C(17:0)	0.56	33	0.58	32

[a] Order parameters are: $\langle P_2(\cos \alpha)\rangle = (1/2)(3\langle \cos^2 \alpha\rangle - 1$, where angular brackets indicate an ensemble average.

Table 4: Order Parameter, $\langle P_2(\cos \theta_{ch})\rangle$, of Lipid chains in Aligned Membranes of Disaturated Phosphatidylcholines, diC(n_C:0)PtdCho, Containing OmpG, in the Gel and Fluid Phases and (tilt, θ_{ch}) of the Chains in the Gel Phase[a]

	$\langle P_2(\cos \theta_{ch,s})\rangle$ (2850 cm^{-1})[b]		$\langle P_2(\cos \theta_{ch,as})\rangle$ (2919 cm^{-1})[c]	
C(n_C:0)	gel	fluid	gel	fluid
C(12:0)		0.35		0.38
C(13:0)	0.46(37°)[a]	0.38	0.46(37°)[a]	0.38
C(14:0)	0.53(34°)[a]	0.33	0.51(35°)[a]	0.33
C(15:0)	0.60(31°)[a]	0.30	0.51(35°)[a]	0.33
C(16:0)	0.46(37°)[a]	0.35	0.51(35°)[a]	0.38
C(17:0)	0.58(32°)[a]	0.41	0.53(34°)[a]	0.35

[a] Chain order parameters are defined by $\langle P_2(\cos \theta_{ch})\rangle = (1/2)(3\langle \cos^2 \theta_{ch}\rangle - 1)$. Chain tilt, θ_{ch}, in the gel phase is given in parentheses. [b] Deduced from the dichroism of the CH_2 symmetric stretch band at 2850 cm^{-1}. [c] Deduced from the dichroism of the CH_2 antisymmetric stretch band at 2919 cm^{-1}.

where angular brackets indicate an ensemble average. Consistent values for $\langle P_2(\cos\theta_{ch})\rangle$ are obtained from the symmetric and antisymmetric stretch bands. The order parameters in the fluid phase are smaller than those in the gel phase, corresponding to chain fluidization; these values then represent the mean order of the individual chain segments that are undergoing rotational isomerism. In the gel phase, the values obtained for θ_{ch} correspond to the tilt of the long axis of the nearly all-*trans* chains. For comparison, the static tilt of the chains of disaturated phosphatidylcholines in gel-phase bilayers that is determined from X-ray diffraction lies in the range $\theta_{ch} = 30-35°$ (*36*). The values of θ_{ch} that are derived for the gel-phase membranes in Table 4 are close to this range and therefore indicate that the reconstituted membranes that contain OmpG are reasonably well aligned.

DISCUSSION

Stoichiometry of Lipid Interaction. It is anticipated that the lipid stoichiometry of OmpG is related to the size, that is, number of strands, of the β-barrel. The number of lipids that can be accommodated at one intramembranous surface of a β-sheet (or a large or flattened β-barrel) with n_β strands is (*12*):

$$N_b = n_\beta D_\beta/(d_{ch}\cos\beta) \quad (6)$$

where $D_\beta = 0.47$ nm is the separation between adjacent strands, and $d_{ch} = 0.48$ nm is the width of a lipid chain. With the strand tilt $\beta = 44 \pm 0.7°$ from IR dichroism, a stoichiometry of $N_b = 19.1 \pm 0.2$ is predicted, which is close to the measured stoichiometry of $N_b = 20 \pm 1$ from spin-label EPR.

Selectivity of Lipid−protein Interaction. OmpG displays very limited selectivity of interaction between the different lipids tested, with the exception of diacylglycerol (see Table 1). The low polarity and deeper location within the bilayer of this latter lipid (*32*) is responsible for the apparent anomaly.

The short turns that connect the transmembrane strands on the periplasmic side of OmpG are almost exclusively acidic: including the N-terminal, there are 9 acidic residues and only two basic residues in the vicinity of the lipid polar headgroups (*1*). In the periplasmic leaflet, there is therefore no electrostatic basis for a selective interaction with anionic lipids, such as is found with many other transmembrane proteins (*9, 11, 37*). On the extracellular side, there are also only 3 basic residues that face outward from the β-barrel and are located in the region of the lipid headgroups (*1*). On the other hand, there is a high concentration of acidic residues in this region and in the extracellular loops. The electrostatic surfaces that are shown in Figure 8 reflect this preponderance of negatively charged residues and illustrate why OmpG does not display a selectivity for anionic lipids.

β-Strand Configuration. Measurements from the amide infrared dichroism yield a consistent value of $\beta = 44.0 \pm 0.7°$ for the tilt of the β-strands in the different phosphatidylcholine lipid hosts. For a β-barrel with n_β strands, the tilt is related directly to the shear number, S, of the barrel by (*38, 39*):

$$\tan\beta = \frac{h}{D_\beta}\frac{\sin(\pi/n_\beta)}{\pi}S \quad (7)$$

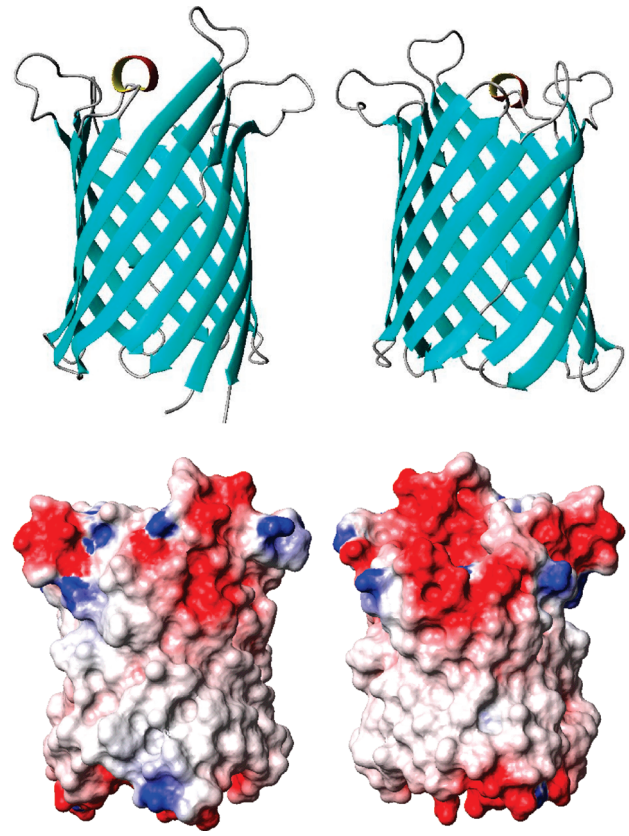

FIGURE 8: Ribbon diagrams and electrostatic surfaces of OmpG (PDB code 2F1C (*1*)), prepared with MolMol (*54*). In the electrostatic coloring, blue is positive, red is negative, and white is apolar. Back and front views of OmpG are shown.

where h is the rise per residue along the strand ($h/D_\beta = 0.719 \pm 0.022$). This predicts a value of $\beta = 42.5 \pm 0.9°$ for OmpG, which has a shear number $S = 18$ (*1*). The theoretical estimate is quite close to the value measured here from infrared dichroism.

The values obtained for the strand tilt, β, from the polarized IR measurements can be used to obtain estimates of the sheet twist, θ, and the strand coiling, ε, by using expressions derived for idealized β-barrels (*39, 40*):

$$\theta = \frac{\theta_o + \frac{2\pi}{n_\beta}\left[\left(\frac{h}{D_\beta}\right)^2\frac{\cos\beta}{\tan\beta} + \sin\beta\right]}{\left(\frac{h}{D_\beta}\right)^2\frac{1}{\tan^2\beta} + \frac{1}{\cos^2\beta}} \quad (8)$$

and

$$\varepsilon = \left(\frac{h}{D_\beta}\right)\left(\frac{2\pi}{n_\beta} - \frac{\theta}{\sin\beta}\right)\cos\beta \quad (9)$$

where $\theta_o = -3.4°$ is the twist in a unstrained sheet of long strands. This yields values for the twist of $\theta = 10°$ and for the coiling of $\varepsilon = 6°$, from the IR dichroism of OmpG in lipid membranes. Previous work has shown that eqs 7 and 8 are capable of predicting the sheet twist and strand coiling with good precision (*8, 39*).

Hydrophobic Span and Matching. The crystal structure of the OmpG transmembrane barrel shows that the hydrophobic belt and aromatic girdles comprise an average of 4.7 outward-facing residues in the 14 strands of the β-barrel (*1*). With a mean strand tilt of 44° from IR dichroism, the transmembrane thickness of this hydrophobic stretch is

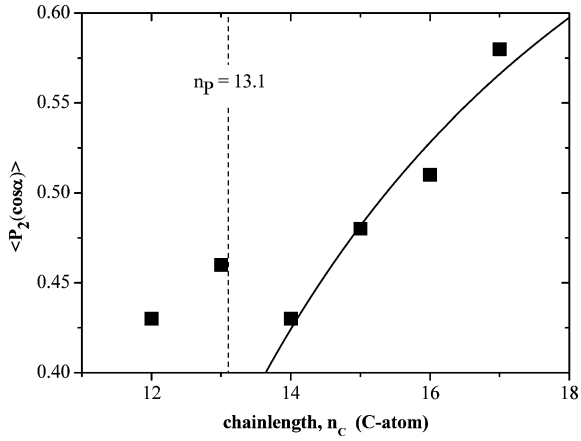

FIGURE 9: Dependence of the order parameters $\langle P_2(\cos\alpha)\rangle$ of OmpG on lipid chainlength, n_C, of the fluid-phase diC(n_C:0)PtdCho membrane in which OmpG is incorporated. The vertical dashed line corresponds to the lipid chainlength, n_P, that gives hydrophobic matching with OmpG. The solid line is a nonlinear least-squares fit of the chainlength dependence $P_2 \sim[1 - B/(n - 1)^2] \times f$ (where $n > n_P$) that is expected for elastic bending fluctuations of the membrane (*47*). The optimized value of $f = 0.84 \pm 0.04$ allows for the fact that the sample may not be perfectly aligned.

therefore predicted to be $9.4 \times h \cos\beta = 2.3$ nm. The OPM database (*41*), which determines the energetics of inserting the protein crystal structure in an implicit hydrophobic membrane (*42*) with experimentally determined boundary function (*43*), reports hydrophobic thicknesses of 2.30−2.37 ± 0.15 nm for OmpG. The simple geometrical estimate is in good agreement with this value.

Using recently refined X-ray data for phosphatidylcholine bilayers, the above value for the hydrophobic span of OmpG corresponds to the hydrophobic core of a diC(n_C:0)PtdCho membrane with an effective chainlength of $n_P = 13.1$ (*44, 45*). This corresponds to the point above which the OmpG dichroic ratios (Figure 7) and order parameters (Table 3) increase monotonically with increasing lipid chainlength. It also correlates with the chainlength above which OmpA is unable to insert spontaneously into large unilamellar vesicles of phosphatidylcholine (*46*).

The increasing orientational order, $\langle P_2(\cos\alpha)\rangle$, or decreasing tilt, α, of the β-barrel with increasing chainlength, n_C, of the host diC(n_C:0)PtdCho lipid has been interpreted previously in terms of hydrophobic matching (*8*), and additionally of elastic bending fluctuations of the membrane, which modulate the orientation of the protein relative to the ATR substrate (*47*). Figure 9 shows the chain-length dependence of the OmpG barrel order parameters. They remain approximately constant up to the region of hydrophobic matching around $n_P = 13.1$. For these shorter chain lengths, the protein may respond to hydrophobic mismatch by tilting slightly, most probably in a dynamic fashion. Beyond this, the solid line represents a nonlinear, least-squares fit to the measured order parameters with a chain-length dependence that is predicted for elastic bending fluctuations of the lipid membrane (*47*). This is capable of describing the chain-length dependence reasonably well, without an appreciable degree of additional static or dynamic disorder (see Figure 9).

Comparison with Other Outer-Membrane Proteins. It is of considerable interest to compare the present results with those from other monomeric β-barrel membrane proteins (*7, 8*).

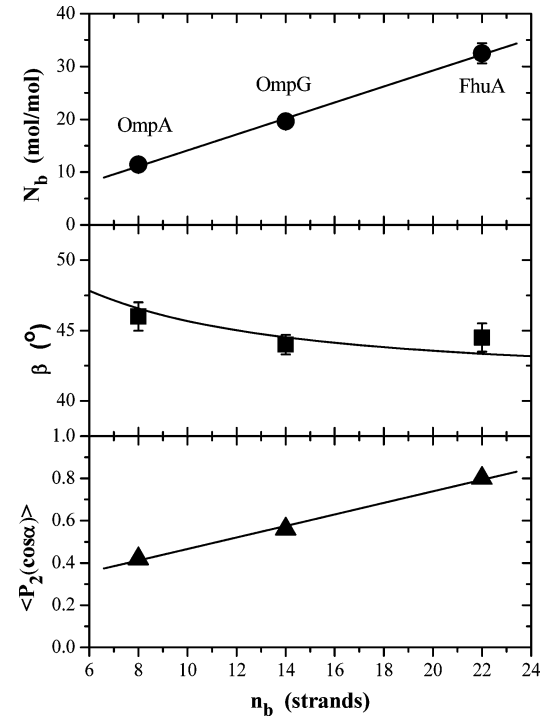

FIGURE 10: Dependence on the number of β-strands, n_β, of (top panel, ●) the motionally restricted lipid stoichiometry, N_b; (center panel, ■) β-strand tilt, β; and (bottom panel, ▲) β-barrel order parameter, $\langle P_2(\cos\alpha)\rangle$, in fluid-phase diC(17:0)PtdCho for the monomeric *E. coli* outer membrane proteins OmpG (this work), OmpA, and FhuA (*7, 8*). Straight lines are linear regressions; for definition of the curved line, see text.

OmpG has $n_\beta = 14$ β-strands with a shear number $S = 18$, which is a size that lies between that of the other monomeric β-barrel proteins, OmpA ($n_\beta = 8$; $S = 10$) and FhuA ($n_\beta = 22$; $S = 24$).

Figure 10 shows the dependence of different parameters on the number of strands, n_β, in the β-barrel. The number of motionally restricted lipids increases linearly with n_β (Figure 10, top), as is predicted by eq 6 if the strand tilt remains approximately constant (cf. Figure 10, middle). The gradient $dN_b/dn_\beta = 1.5 \pm 0.1$ that is obtained by linear regression also is close to that predicted from eq 6: $dN_b/dn_\beta \sim \sec\beta \approx 1.4$. The strand tilt, β, varies relatively little between the three proteins (Figure 10, middle), less than would be predicted by eq 7. The solid line in Figure 10 (middle) is the prediction of eq 7 for $S = n_\beta + 2$ taking $h/D_\beta = 0.741$, with a constant offset of +4.5° added. Note that, whereas $S = n_\beta + 2$ for both OmpA and FhuA, $S = n_\beta + 4$ for OmpG. This might account for part of the discrepancy with eq 7. In addition, as noted previously (*8*), the strand tilts from IR dichroism tend to be larger than those from the crystal structures with which the value of h/D_β in eq 7 is standardized (*39*). This may result from a slight relaxation of the barrel structure in lipid membranes, relative to the packing of the protein in the crystal.

The bottom panel of Figure 10 shows the order parameters of the three proteins that are determined at the same temperature in the fluid phase of the lipid with longest chains, diC(17:0)PtdCho. The ordering of the barrel axis increases progressively with size of the barrel, with FhuA being very highly ordered $\langle P_2(\cos\alpha)\rangle \approx 0.8$. An approximately linear dependence of order parameter on n_β is found. (It should be noted, however, that the dependence on lipid chain length

is steeper for OmpG than it is for OmpA and FhuA.) Correspondingly, the effective angle of tilt increases with decreasing size of the β-barrel, from $\alpha \approx 38°$ for OmpA, via $\alpha \approx 32°$ for OmpG, to $\alpha \approx 21°$ for FhuA.

By and large, the parameters for OmpG lie between those for OmpA and FhuA. This applies also to the twist of the β-sheets and the coiling of the β-strands. The present work with OmpG thus establishes a regularity in the membrane interactions of monomeric β-barrel proteins, which can be used to gain valuable information on other outer membrane proteins of unknown size and/or structure. A possible example is the nonspecific porin FomA, which is the major outer membrane protein of *Fusobacterium nucleatum* (*48*). The structure of FomA is unknown, but has been proposed to be a β-barrel with variously 14 (*49*) or 16 (*50, 51*) antiparallel β-strands. This protein migrates as a monomer in SDS−PAGE, without denaturation prior to electrophoresis, as do OmpG, OmpA, and FhuA (*52*). Therefore, measurements of the type presented in Figure 10 could help to decide between the different models for the β-barrel structure.

ACKNOWLEDGMENT

We thank Frau B. Angerstein for the synthesis of spin-labeled phospholipids.

REFERENCES

1. Subbarao, G. V., and van den Berg, B. (2006) Crystal structure of the monomeric porin OmpG. *J. Mol. Biol. 360*, 750–759.
2. Yildiz, Ö., Vinothkumar, K. R., Goswami, P., and Kühlbrandt, W. (2006) Structure of the monomeric outer-membrane porin OmpG in the open and closed conformation. *EMBO J. 25*, 3702–3713.
3. Conlan, S., Zhang, Y., Cheley, S., and Bayley, H. (2000) Biochemical and biophysical characterization of OmpG: a monomeric porin. *Biochemistry 39*, 11845–11854.
4. Misra, R., and Benson, S. A. (1989) A novel mutation, *cog*, which results in production of a new porin protein (OmpG) of *Escherichia coli* K-12. *J. Bacteriol. 171*, 4111.
5. Fajardo, D. A., Cheung, J., Ito, C., Sugawara, E., Nikaido, H., and Misra, R. (1998) Biochemistry and regulation of a novel *Escherichia coli* K-12 porin protein, OmpG, which produces unusually large channels. *J. Bacteriol. 180*, 4452–4459.
6. Conlan, S., and Bayley, H. (2003) Folding of a monomeric porin, OmpG, in detergent solution. *Biochemistry 42*, 9453–9465.
7. Ramakrishnan, M., Pocanschi, C. L., Kleinschmidt, J. H., and Marsh, D. (2004) Association of spin-labelled lipids with β-barrel proteins from the outer membrane of *Escherichia coli*. *Biochemistry 43*, 11630–11636.
8. Ramakrishnan, M., Qu, J., Pocanschi, C. L., Kleinschmidt, J. H., and Marsh, D. (2005) Orientation of β-barrel proteins OmpA and FhuA in lipid membranes. Chainlength dependence from infrared dichroism. *Biochemistry 44*, 3515–3523.
9. Marsh, D., and Horváth, L. I. (1998) Structure, dynamics and composition of the lipid-protein interface. Perspectives from spin-labelling. *Biochim. Biophys. Acta 1376*, 267–296.
10. Marsh, D. (1999) Spin label ESR spectroscopy and FTIR spectroscopy for structural/dynamic measurements on ion channels. *Methods Enzymol. 294*, 59–92.
11. Marsh, D. (2008) Protein modulation of lipids, and vice-versa, in membranes, *Biochim. Biophys. Acta*, doi:10.1016/j.bbamem.2008.01.015.
12. Marsh, D. (1997) Stoichiometry of lipid-protein interaction and integral membrane protein structure. *Eur. Biophys. J. 26*, 203–208.
13. Marsh, D. (1997) Dichroic ratios in polarized Fourier transform infrared for nonaxial symmetry of β-sheet structures. *Biophys. J. 72*, 2710–2718.
14. Hubbell, W. L., and McConnell, H. M. (1971) Molecular motion in spin-labelled phospholipids and membranes. *J. Am. Chem. Soc. 93*, 314–326.
15. Marsh, D. and Watts, A. (1982) Spin-Labeling and Lipid-Protein Interactions in Membranes, in *Lipid-Protein Interactions, Vol. 2* (Jost, P. C., and Griffith, O. H., Eds.) pp 53−126, Wiley-Interscience, New York.
16. Qu, J., Mayer, C., Behrens, S., Holst, O., and Kleinschmidt, J. H. (2007) The trimeric periplasmic chaperone Skp of *Escherichia coli* forms 1:1 complexes with outer membrane proteins via hydrophobic and electrostatic interactions. *J. Mol. Biol. 374*, 91–105.
17. Lowry, O. H., Rosebrough, N. J., Farr, L., and Randall, R. J. (1951) Protein measurement with the Folin phenol reagent. *J. Biol. Chem. 193*, 265–275.
18. Marsh, D. (1982) Electron Spin Resonance: Spin Label Probes, in *Techniques in Lipid and Membrane Biochemistry, Vol. B4/II* (Metcalfe, J. C., and Hesketh, T. R., Eds.) pp B426/1−B426/44, Elsevier, New York.
19. Kóta, Z., Páli, T., and Marsh, D. (2004) Orientation and lipid-peptide interactions of gramicidin A in lipid membranes: polarized ATR infrared spectroscopy and spin-label electron spin resonance. *Biophys. J. 86*, 1521–1531.
20. Marsh, D. (1983) Spin label answers to lipid-protein interactions. *Trends Biochem. Sci. 8*, 330–333.
21. Pates, R. D., and Marsh, D. (1987) Lipid mobility and order in bovine rod outer segment disk membranes. A spin-label study of lipid-protein interactions. *Biochemistry 26*, 29–39.
22. Watts, A., Davoust, J., Marsh, D., and Devaux, P. F. (1981) Distinct states of lipid mobility in bovine rod outer segment membranes. Resolution of spin label results. *Biochim. Biophys. Acta 643*, 673–676.
23. Esmann, M., and Marsh, D. (1985) Spin-label studies on the origin of the specificity of lipid-protein interactions in Na^+,K^+-ATPase membranes from *Squalus acanthias*. *Biochemistry 24*, 3572–3578.
24. Horváth, L. I., Brophy, P. J., and Marsh, D. (1988) Exchange rates at the lipid-protein interface of myelin proteolipid protein studied by spin-label electron spin resonance. *Biochemistry 27*, 46–52.
25. Horváth, L. I., Brophy, P. J., and Marsh, D. (1988) Influence of lipid headgroup on the specificity and exchange dynamics in lipid-protein interactions. A spin label study of myelin proteolipid apoprotein-phospholipid complexes. *Biochemistry 27*, 5296–5304.
26. Horváth, L. I., Brophy, P. J., and Marsh, D. (1993) Exchange rates at the lipid-protein interface of the myelin proteolipid protein determined by saturation transfer electron spin resonance and continuous wave saturation studies. *Biophys. J. 64*, 622–631.
27. Ryba, N. J. P., Horváth, L. I., Watts, A., and Marsh, D. (1987) Molecular exchange at the lipid-rhodopsin interface: spin-label electron spin resonance studies of rhodopsin-dimyristoyl phosphatidylcholine recombinants. *Biochemistry 26*, 3234–3240.
28. Sachse, J.-H., King, M. D., and Marsh, D. (1987) ESR determination of lipid diffusion coefficients at low spin-label concentrations in biological membranes, using exchange broadening, exchange narrowing, and dipole-dipole interactions. *J. Magn. Reson. 71*, 385–404.
29. King, M. D., Sachse, J.-H., and Marsh, D. (1987) Unconstrained optimization method for interpreting the concentration and temperature dependence of the linewidths of interacting nitroxide spin labels. Application to the measurement of translational diffusion coefficients of spin-labeled phospholipids in membranes. *J. Magn. Reson. 72*, 257–267.
30. Meier, P., Sachse, J.-H., Brophy, P. J., Marsh, D., and Kothe, G. (1987) Integral membrane proteins significantly decrease the molecular motion in lipid bilayers: a deuteron NMR relaxation study of membranes containing myelin proteolipid apoprotein. *Proc. Natl. Acad. Sci. U.S.A. 84*, 3704–3708.
31. Brotherus, J. R., Griffith, O. H., Brotherus, M. O., Jost, P. C., Silvius, J. R., and Hokin, L. E. (1981) Lipid-protein multiple binding equilibria in membranes. *Biochemistry 20*, 5261–5267.
32. Schorn, K., and Marsh, D. (1996) Lipid chain dynamics and molecular location of diacylglycerol in hydrated binary mixtures with phosphatidylcholine: spin label ESR studies. *Biochemistry 35*, 3831–3836.
33. Miyazawa, T. (1960) Perturbation treatment of the characteristic vibrations of polypeptide chains in various configurations. *J. Chem. Phys. 32*, 1647–1652.
34. Liang, B., and Tamm, L. K. (2007) Structure of outer membrane protein G by solution NMR spectroscopy. *Proc. Natl. Acad. Sci. U.S.A. 104*, 16140–16145.
35. Shanmugavadivu, B., Apell, H. J., Meins, T., Zeth, K., and Kleinschmidt, J. H. (2007) Correct folding of the β-barrel of the human membrane protein VDAC requires a lipid bilayer. *J. Mol. Biol. 368*, 66–78.
36. Marsh, D. (1990) *Handbook of Lipid Bilayers* CRC Press, Boca Raton, FL.

37. Esmann, M., and Marsh, D. (2006) Lipid-protein interactions with the Na,K-ATPase. *Chem. Phys. Lipids 141*, 94–104.
38. Chou, K.-C., Carlacci, L., and Maggiora, G. G. (1990) Conformational and geometrical properties of idealized β-barrels in proteins. *J. Mol. Biol. 213*, 315–326.
39. Páli, T., and Marsh, D. (2001) Tilt, twist and coiling in β-barrel membrane proteins: relation to infrared dichroism. *Biophys. J. 80*, 2789–2797.
40. Marsh, D. (2000) Infrared dichroism of twisted β-sheet barrels. The structure of *E. coli* outer membrane proteins. *J. Mol. Biol 297*, 803–808.
41. Lomize, M. A., Lomize, A. L., Pogozheva, I., and Mosberg, H. I. (2006) OPM: orientations of proteins in membranes database. *Bioinformatics 22*, 623–625.
42. Lomize, A. L., Pogozheva, I. D., Lomize, M. A., and Mosberg, H. I. (2006) Positioning of proteins in membranes: a computational approach. *Protein Sci. 15*, 1318–1333.
43. Marsh, D. (2001) Polarity and permeation profiles in lipid membranes. *Proc. Natl. Acad. Sci. U.S.A. 98*, 7777–7782.
44. Marsh, D., Jost, M., Peggion, C., and Toniolo, C. (2007) Lipid chainlength dependence for incorporation of alamethicin in membranes: EPR studies on TOAC-spin labelled analogues. *Biophys. J. 92*, 4002–4011.
45. Marsh, D. (2008) Energetics of hydrophobic matching in lipid-protein interactions, *Biophys. J.*, *94*, 3996–4013.
46. Kleinschmidt, J. H., and Tamm, L. K. (2002) Secondary and tertiary structure formation of the β-barrel membrane protein OmpA is synchronized and depends on membrane thickness. *J. Mol. Biol. 324*, 319–330.
47. Marsh, D., Shanmugavadivu, B., and Kleinschmidt, J. H. (2006) Membrane elastic fluctuations and the insertion and tilt of β-barrel proteins. *Biophys. J. 91*, 227–232.
48. Kleivdal, H., Benz, R., and Jensen, H. B. (1995) The *Fusobacterium nucleatum* major outer-membrane protein (FomA) forms trimeric, water-filled channels in lipid bilayer membranes. *Eur. J. Biochem. 233*, 310–316.
49. Puntervoll, P., Ruud, M., Bruseth, L. J., Kleivdal, H., Høgh, B. T., Benz, R., and Jensen, H. B. (2002) Structural characterization of the fusobacterial non-specific porin FomA suggests a 14-stranded topology, unlike the classical porins. *Microbiology 148*, 3395–3403.
50. Bolstad, A. I., Tommassen, J., and Jensen, H. B. (1994) Sequence variability of the 40-kDa outer membrane proteins of *Fusobacterium nucleatum* strains and a model for the topology of the proteins. *Mol. Gen. Genet. 244*, 104–110.
51. Bolstad, A. I., Høgh, B. T., and Jensen, H. B. (1995) Molecular characterisation of a 40-kDa outer membrane protein, FomA, of *Fusobacterium periodonticum* and comparison with *Fusobacterium nucleatum*. *Oral Microbiol. Immunol. 10*, 257–264.
52. Pocanschi, C. L., Apell, H. J., Puntervoll, P., Høgh, B., Jensen, H. B., Welte, W., and Kleinschmidt, J. H. (2006) The major outer membrane protein of *Fusobacterium nucleatum* (FomA) folds and inserts into lipid bilayers via parallel folding pathways. *J. Mol. Biol. 355*, 548–561.
53. Marsh, D. (1999) Quantitation of secondary structure in ATR infrared spectroscopy. *Biophys. J. 77*, 2630–2637.
54. Koradi, R., Billeter, M., and Wüthrich, K. (1996) MOLMOL: a program for display and analysis of macromolecular structures. *J. Mol. Graphics 14*, 51–55.

BI800203G